BULLETIN OF THE POLISH ACADEMY OF SCIENCES
TECHNICAL SCIENCES, Vol. 69(5), 2021, Article number: e138567
DOI: 10.24425/bpasts.2021.138567

Dynamics of autonomous rock electromagnetic radiation measurement instrumentation

Remigiusz MYDLIKOWSKI[1*] **and Krzysztof MANIAK**[2]

[1] Wroclaw University of Science and Technology, Faculty of Electronics, Photonics and Microsystems, ul. Janiszewskiego 11/17, 50-372 Wrocław, Poland

[2] National Institute of Telecommunications, ul. Szachowa 1, 04-894 Warsaw, Poland

Abstract. The paper analyzes the operation of innovative composite measurement instrumentation for spontaneous electromagnetic emission. The designed receiver measures and records both components of the EM field emitted by rocks subjected to increased mechanical stress. The range of signals transmitted by the receiver system and its dynamics were determined. A receiver was used to observe electromagnetic signals generated during a hard coal sample crushing in laboratory conditions. Test results confirmed the high dynamic range of the system at 98 dB and the ability to observe signals over a range of frequencies up to 50 kHz. The experimental results confirm the signal bandwidth characteristic of coal mine EM field emission obtained in earlier studies. The constructed autonomous receiver can be used in mine workings as a complementary warning system for emerging mine hazards.

Key words: electromagnetic field; EM receiver; rock destruction; dynamics of operation.

1. INTRODUCTION

Mine disasters are constantly related to mining exploitation. Nowadays, despite significant development of technology and knowledge about work safety, there are still disasters involving severe damage to the life or health of miners and destruction of technical infrastructure [1, 2]. Mine collapses cause most disasters. Mine collapses occur in places of accumulation of mechanical stresses in the workings and weakening of the rock structure. From the safety point of view, it is important to detect the first symptoms of such a developing phenomenon, which initially include seismic microshocks and rock micro-cracks. The seismic method is the oldest and most widely used method for recording mining hazards that can lead to collapse [3]. The use of a network of geophones allows for continuous monitoring of seismic events in a mine. Early detection of a hazard allows deciding on the evacuation of miners. Geophones of different designs are used to detect these phenomena [4]. The network of such sensors is located at critical points of the mine, from which the signals are led to the monitoring center. Gas explosions or ignition of coal dust are equally common threats as mine collapses [5]. For this purpose, the mines have special sensitive sensors that detect flammable elements in the air. Mine equipment is safe from sparks thanks to specialized enclosures. Cases of mine gas ignition from sparks emitted during the crushing of rocks with high content of piezoelectric materials are also observed [6]. Most of such disasters are related to coal mining.

Various strategies are taken to identify possible disaster factors and counteracting their effects [7, 8]. New methods are being sought to predict mine disasters in advance to enable the efficient evacuation of miners. One of the new trends in forecasting mine disasters is the recording and analyzing anomalous electromagnetic field radiation by stressed rocks, including hard coal. Many laboratory tests are carried out on the essence of this phenomenon [9–11]. However, fewer reports are presenting specific hardware solutions for recording and analyzing this phenomenon in mines. It has been noted that the temporal electrical waveforms obtained during testing have the character of a bundle of fading impulses [12], whose frequency spectrum is continuous. To determine the intensity of the generated spontaneous electromagnetic field, the authors provide general test results. To interpret the results, for example, the activity of the pulses per unit time or the value of the DC voltage corresponding to the instantaneous values of the pulse amplitude are defined. Relative units are also often given. In this case, it is difficult to unambiguously deduce which field strengths the researchers were dealing with.

In each case, frequency bands of enhanced EM emission can be distinguished for each rock sample tested [13]. As a result of an increase in the internal mechanical stresses of the rock mass, spontaneous emission of weak EM fields occurs. Similar results were obtained in studies on active landslides. A positive correlation of the recorded electromagnetic field emission with geological measurements of landslide activity was obtained. In particular, with the commonly used inclinometric method [14]. Many researchers report anomalously high levels of EM fields accompanying a coal mine collapse [15–17]. These phenomena occur even a few hours before the disaster that is to take place, i.e., in advance, which enables an efficient evacuation of miners from the place of the threat of a collapse.

The device presented in this paper is part of the trend of searching for equipment that allows practical use of electro-

*e-mail: remigiusz.mydlikowski@pwr.edu.pl

Manuscript submitted 2021-03-09, revised 2021-05-26, initially accepted for publication 2021-08-13, published in October 2021

magnetic field emission from rocks subjected to increased mechanical stress. The receiver should provide insight into the nature of EM fields occurring during mine operation.

2. MECHANISM OF EM EMISSION FROM ROCK

For many years, spontaneous electromagnetic field emission formation under the influence of increased rock stress has been described in the literature [18]. This process is recorded during earthquakes [19], active movements of landslides or collapses of mine rock masses. The genesis of electromagnetic field emission is defined in several ways. The most important of them are piezoelectric phenomena and EM field generation due to the formation of microcracks.

2.1. Piezoelectric effect

This effect is particularly significant in rocks containing fractions rich in piezoelectric crystals, e.g. sandstones, gravels, etc. It applies to rocks built entirely of crystals and rocks of a mixed structure containing piezoelectric material in their partial admixtures. The character of the emission strongly depends on the type of material being destroyed and the mode of interaction of the destructive forces. The most common naturally occurring piezoelectric minerals include quartz, tourmaline, sphalerite, nepheline. The piezoelectric effect is also observed in minerals with dielectric and semiconducting properties, such as selenium, tellurium, greenockite, zincite.

The activation of the piezoelectric effect occurs due to internal stresses, pressure and friction occurring during the development of stresses in the rock material.

The piezoelectric effect is observed in dielectric media of anisotropic structure, having a suitable crystallographic structure.

These relations are described by the following equations [20]:

$$S_{ij} = s^E_{ijkl} T_{kl} + d_{kij} E_k \,, \tag{1}$$

$$D_i = d_{ikl} T_{kl} + \varepsilon^T_{ik} E_k \,, \tag{2}$$

where:

S_{ij} – mechanical deformation component,
T_{kl} – component of mechanical stress,
E_k – component of the electric field,
D_i – electric displacement component.

It follows from relation (2) that the change of electric displacement component D is proportional to the stress T forced on the sample of a piezoelectric crystal, in the absence of internal self-stress of the sample (so-called reverse piezoelectric phenomenon). The phenomenon described by relation (1), which leads to the appearance of internal stresses in the crystal under the influence of applied electric field E (so-called simple piezoelectric phenomenon), is also observed. The abrupt change of the electric displacement component D, which is the source of broadband electromagnetic fields, is caused by changes of stresses in the material under study and the rock crushing phenomenon.

2.2. Micro-cracks in the rock structure

The process of emission of electromagnetic fields, mainly from rocks without quartz crystals in their structure, which include, among others, hard coal, is explained on the example of a network of micro-cracks formed under the influence of compressive force, whose fractures are performed by oscillatory vibrations [21–23]. This mechanism concerns micro-cracks of sizes from hundredths to several millimetres [24]. An electric diagram of a single micro-crack is shown in Fig. 1 [25]. As can be seen, the system is composed of a capacitor with a capacity of C, the covers of which perform vibrations damped around the stable position d. One cover is grounded, and the other one is loaded with resistance R.

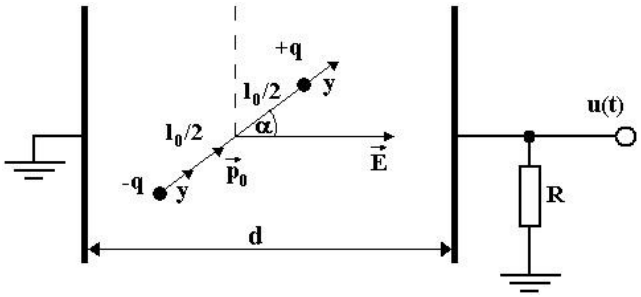

Fig. 1. Electrical schematics of micro-cracks [25]

Assuming that the edges of micro-cracks are endowed with a heteronymous electrical charge [26] and starting from the law of conservation of energy, we can write [25] for the micro-cracks formed in the rock structure:

$$\vec{E}\left(\sum_{k=1}^{N} q_k \vec{v}_k\right) \mathrm{d}t = Ri^2\,\mathrm{d}t + Cu\,\mathrm{d}u \,, \tag{3}$$

where:

q_k – elementary electric charge on the edges of the crack,
$\vec{v}_k$ – speed of charge propagation,
$\vec{E}$ – the intensity of the electric field,
$Ri^2\,\mathrm{d}t$ – energy exhaled on the load resistance,
$Cu\,\mathrm{d}u$ – energy between the plates of the capacitor,
N – the number of electric charges accumulated between the covers of the capacitor.

The left side of equation (3) represents energy unleash during the creation of micro-crack.

Equation (3) can be rewritten in the form:

$$\frac{1}{C}\vec{E}_1\left(\sum_{k=1}^{N} q_k \vec{v}_k\right) = \frac{u}{\tau} + \frac{\mathrm{d}u}{\mathrm{d}t} \,, \tag{4}$$

where:

$$\vec{E}_1 = \frac{\vec{E}}{u} \,, \quad \tau = RC.$$

A pair of static charges $-q$, $+q$ at a distance of l_0 forms an electric dipole with a dipole moment $\vec{p}_0$ (Fig. 1). As a result of

damping of the gap edges, the load changes its spatial position over time according to the relation:

$$y(t) = y_0 e^{-\delta t} \sin(\omega t), \tag{5}$$

where:

δ, ω – constants of damped vibration,

y_0 – charge off position.

Eventually, the differential equation that describes the process of the emission of an electromagnetic field with the vibration of micro-crack (5) can be written:

$$\frac{\mathrm{d}u}{\mathrm{d}t} + \frac{u}{\tau} = a e^{-bt} \sin(\omega t + \varphi), \tag{6}$$

where:

$$a = \frac{2 \cdot q_0 \cdot v_0}{C \cdot d},$$

$$b = \delta + \beta,$$

$$\tan(\varphi) = -\frac{\omega}{\delta},$$

β – decay charge constant,

d – the distance between plates of a capacitor (gap width),

α – angle between vector of electric field intensity $\vec{E}$ and direction of charges movement.

Finally, the voltage present on the plates of the capacitor can be expressed [25]:

$$u(t) = \sum_{i=1}^{2} u_i(t) = U_0 e^{-t/\tau} - \frac{a e^{-bt}}{\sqrt{\omega_0^2 + \omega^2}} \sin(\omega t + \varphi), \tag{7}$$

where:

U_0 – integrate constant.

The DC voltage component $u_1(t)$ corresponds to the discharge of the capacitor by a resistance R with a time constant $\tau = RC$. The alternating current component $u_2(t)$ corresponds to vibrations damped by micro-cracked walls. For example, for samples of chalk and ceramics, the emission spectrum of electric fields is in the range of $10^3 \div 10^7$ Hz [24]. Microcracks also form in coal in addition to the natural pores in the coal structure [27].

The coexistence of mechanisms of electromagnetic emission from rock samples through the generation of micro-cracks and piezoelectric effect is also indicated, which is discussed in the example of granite samples [28].

3. LABORATORY TEST STAND FOR EM FIELD FROM ROCKS

The study of spontaneous electromagnetic field emission signals from rock samples was carried out at the test stand in Fig. 2. At this test stand, the rock sample was subjected to an increasing compressive force by the jaws of a press with a maximum force of 450 kN. Different rates of force increment were tested from 100N/s to 40 kN/s by observing the EM pulses generated. As the rate increased, an increase in the number of EM pulses generated was observed. In each of the tests associated with the rate of force build-up, the spectrum of pulses obtained ranged from hundreds of Hz to 30-40 kHz. In order to ensure proper observation of the phenomenon of generated EM emission pulses during the formation of microcracks and the final destruction of the rock samples, an optimum force increment rate of 1 kN/s was established. This speed allows the observation of the fully developing process of rock destruction without missing important phases of the phenomenon that may occur when the process of mixing is too slow or too fast.

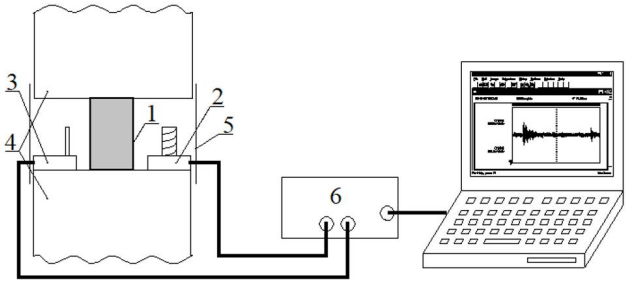

Fig. 2. Laboratory stand for testing electromagnetic fields generated by rock samples: 1 – test sample, 2 – magnetic field sensor, 3 – electric field sensor, 4 – hydraulic press, 5 – electromagnetic screen, 6 – measuring card

Separate receivers for the electric E and magnetic H components of the EM field were placed at a close distance to the test sample. For isolation from external interference, the measuring receivers, together with the tested rock sample, were shielded by a screen connected to the grounding of the test stand. Steel shielding was used to reduce the influence of the magnetic component of external interference and parallel copper sheet shielding to reduce external electric fields. Such a complex shield enables independence from external interference over a wide frequency spectrum. The effectiveness of the shielding increases as the interference frequency increases.

During the experiments, samples of coal, sandstone, dolomite and magnesite were subjected to destruction. Samples from mine and rock boreholes were cut to a height of 5 cm. In order to compensate for the unevenness of the samples and evenly distribute the compressive forces, soft wood was placed between the test sample and the jaws of the press. The computer on the test stand recorded the amplitudes of the obtained signals of the EM field components [13]. The spectral distribution of the signals was further analyzed. The spectra of the signals for the different types of rocks studied were within the frequency range up to 100 kHz. Important spectral bars were observed in the range up to several kHz.

4. AUTONOMOUS ROCK ELECTROMAGNETIC RADIATION MEASUREMENT INSTRUMENTATION

From the analysis of research results in laboratory conditions, assumptions were made to build an autonomous measuring receiver. A receiver that could record spontaneous EM emission in real mining conditions.

4.1. Specification of the construction of an autonomous EM field receiver

The design of the autonomous receiver should have the following technical assumptions, which were established after many earlier tests in the laboratory [13]:

- minimum sensitivity at $E_{\min} = 2 \cdot 10^{-4}$ V/m and $H_{\min} = 1.5 \cdot 10^{-5}$ A/m respectively for the electric and magnetic field component receiver,
- recording of useful signals at frequencies from 50 Hz to 50 kHz,
- recording the current value and the peak value of the electromagnetic pulse in real time,
- independent power source for uninterrupted operation of the receiver for a long-term period, e.g. for a month,
- non-volatile memory,
- no interference with other electronic devices installed in the mine,
- immunity to electromagnetic interference occurring in the mine during its operation,
- hermetic and spark-eliminating case.

4.2. Construction of an autonomous receiver

Figure 3a shows a block diagram of rock electromagnetic radiation measurement instrumentation. This schematic contains four essential functional blocks:

1) system for measuring and processing the signal of the electric component of the EM field,
2) system for measuring and processing the signal of the magnetic component of the EM field,
3) control system with an operation algorithm,
4) own energy supply system.

(a)

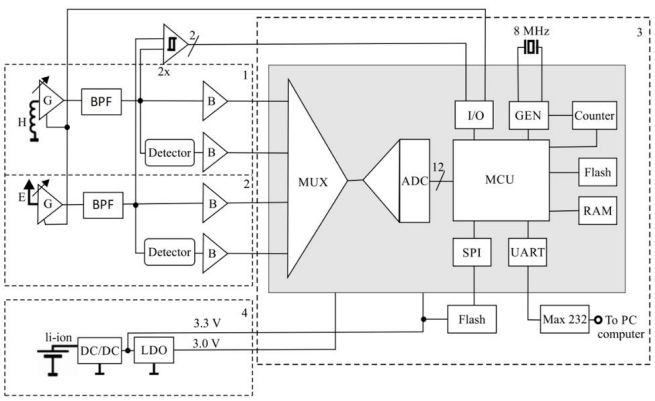

(b)

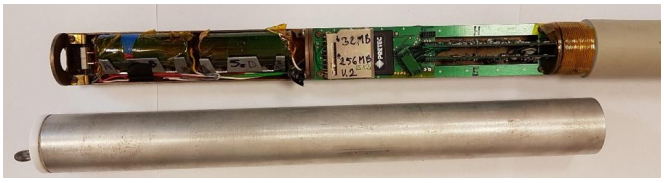

Fig. 3. Composite autonomous EM field receiver. a) block diagram of rock electromagnetic radiation measurement instrumentation, b) inside the receiver unit

To miniaturize the compact design, the complete electromagnetic field receiver was made using SMT technology. The system was divided into three printed circuit boards interconnected by a system of microconnectors. On the base plate, there is a microprocessor with associated circuits and a power supply unit. There are analogue signal processing blocks (of the same electrical construction). These blocks cooperate with antennas receiving the electric component – E and the magnetic component – H of the electromagnetic field.

The view of the receiver's interior is shown in Fig. 3b. After closing the casing, the receiver has the following dimensions: length 500 mm and diameter 40 mm.

The antenna for receiving the electrical component was made as a monopole in the form of a 20 cm long copper rod for which the reference ground is the brass structure of the receiver. The effective h_{ef} height of the antenna as half the geometric length of the rod is equal to 10 cm. Because $h_{ef} \ll \lambda$ the voltage induced in the antenna is [29]:

$$SEM_E = Eh_{ef}\,, \tag{8}$$

where:

E – electric field strength V/m.

The sensor for the magnetic component H is a ferrite rod antenna with a coil wound on it. The voltage induced in the coil of the antenna can be determined from the relationship [30,31]:

$$SEM_A = Z_0 H \frac{2\pi z S \mu}{\lambda}\,, \tag{9}$$

where:

H – magnetic field strength [A/m]

$Z_0 = 120\pi$ *Omega* – wave impedance of free space,

z – number of antenna wire turns,

S – cross section area of antenna coil [m^2]

λ – signal wavelength [m]

μ – the magnetic permeability effective value of the antenna's ferrite core [H/m].

4.3. Analog signal processing block

Blocks 1 and 2 (Fig. 3a) as analogue parts of signal processing for electric and magnetic components are identical in their electrical construction. A simplified scheme of the analogue part of the device is shown in Fig. 4.

The measured signal coming from the electric or magnetic antenna in the form of voltage U_{IN} goes to the input of voltage follower U1. The role of the follower is the impedance matching of the circuit elements. Then the signal is fed to a passive band pass filter consisting of R1, C1, R2, C2 elements. The filter operates in the range of 50 Hz to 50 kHz. It was decided to use the passive filter to reduce the power consumption of the autonomous system [32].

The transmittance of a bandpass filter section depends on:

$$G1 = \frac{j\omega R_2 C_1}{1 + j\omega\left(R_1 C_1 + R_2 C_2 + R_2 C_1\right) - \omega^2 R_1 R_2 C_1 C_2}\,. \tag{10}$$

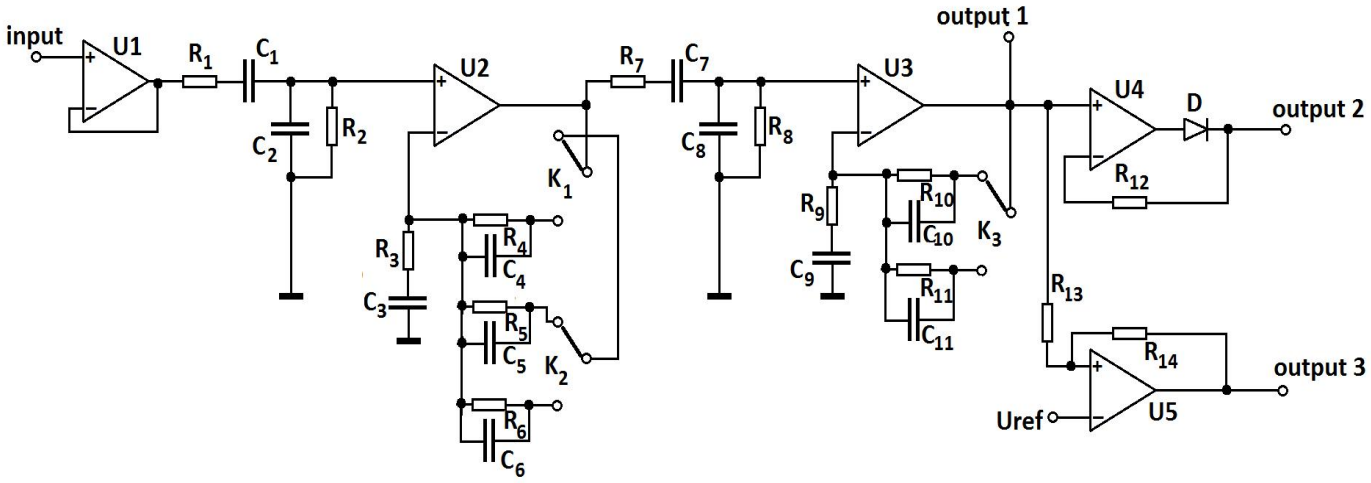

Fig. 4. Analog signal processing block diagram

Operational amplifier U2 with electronically switched keys K1, K2 and K3 is a gain control amplifier, whose gain is determined by the processor depending on the switched element consisting of resistor-capacitor pair. The transmittance of the segment, for the switched key K1 located as on the diagram, shows the relation:

$$G2 = 1 + \frac{j\omega R_4 C_3}{1 - \omega^2 R_3 C_3 R_4 C_4 + j\omega\left(R_3 C_3 + R_4 C_4\right)}. \qquad (11)$$

In order to obtain the appropriate slope of the frequency response and the appropriate dynamics of the system, it was decided to build another filtering and amplifying section (elements with index 7 and 8 and U3).

Change of amplification of the circuit is realized with the cooperation of amplifying units realized on U2, U3 circuits. Appropriate control of the keys K1, K2 and K3 by the processor ensures obtaining discrete resultant amplification, which is the product of individual circuit amplifications, with values: 6, 28, 280, 2800, and 28000 V/V. This process is designed to give more gain to weak signals and less gain to high amplitude waveforms. For example, for the highest sensitivity of the electrical component measurement path, which is achieved for a resultant path gain of 28000 V/V, it can be shown that an antenna output amplitude of 0.1V corresponds to an electric field strength of 1 V/m. The filtered and amplified signal is available at output 1 and is fed through buffer B to the analogue input of the processor. In real time, the obtained waveforms of both field components E and H are recorded and stored for a specified time in the dynamic memory of the processor as the instantaneous value of the signals.

Extending the circuit with additional elements and using an appropriate algorithm controlling the operation of the device makes it possible to record anomalous EM waveforms in permanent memory. The U4 circuit does this in cooperation with the Schottky diode, from which the peak value of the waveform is obtained (output 2). Direct signal and its peak value are stored by the processor on the carrier (SD card) under the condition that at the input of the comparator with hysteresis output 3 (U5 circuit) appears a voltage with amplitude exceeding the value of the reference voltage U_{ref} fixed.

4.4. Determination of the frequency characteristics of an analogue system

Verification measurements of the constructed system were carried out to determine the frequency bandwidth of the device's analogue receiver system. The measurements were performed for different gains (different key positions K1-K3). Figure 5a shows the amplitude characteristics related to the maximum signal Emax. With a gain decrease of 3 dB (i.e. 0.707 of the maximum value), the signals' lower and upper frequency response was determined. These are 49 Hz and 51 kHz, respectively. Outside the frequency response, the amplitude response has a slope of 12 dB/oct, corresponding to a double pole transmittance of the system for the falling edge and a double zero for the rising edge. Effect of using a two-stage bandpass filter (2nd filter order).

Figure 5b shows the phase change of the output signal. The phase changes from $+180^\circ$ to 0° and further to -180°. Such a phase change is characteristic of the dual pole transmittance [31]. The measurements confirm the design of the 2nd-order filter to ensure selective operation of the system beyond the range of the transmitted signal.

4.5. Determination of system dynamics

In order to determine the dynamics of the operation of the autonomous receiver system, the dependence of the output voltage U_{OUT} as a function of the input voltage U_{IN} coming from the antenna was measured. Due to the identity of the electrical system of both paths for measuring the signal from the antenna of the electric and magnetic components of the EM field, a joint analysis was carried out.

Measurements were carried out in the range of average frequencies of the system operation, i.e. the normal operating range of the receiver. The results obtained for $f = 5$ kHz are presented in Table 1.

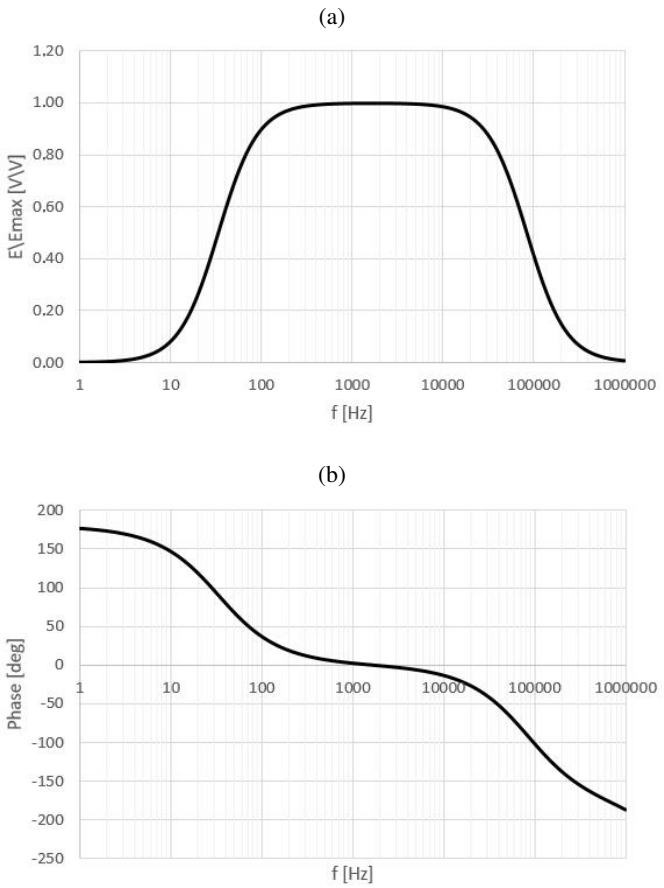

Fig. 5. Frequency characteristics of an electromagnetic field receiver: a) amplitude $E/E_{\max}$, b) phase

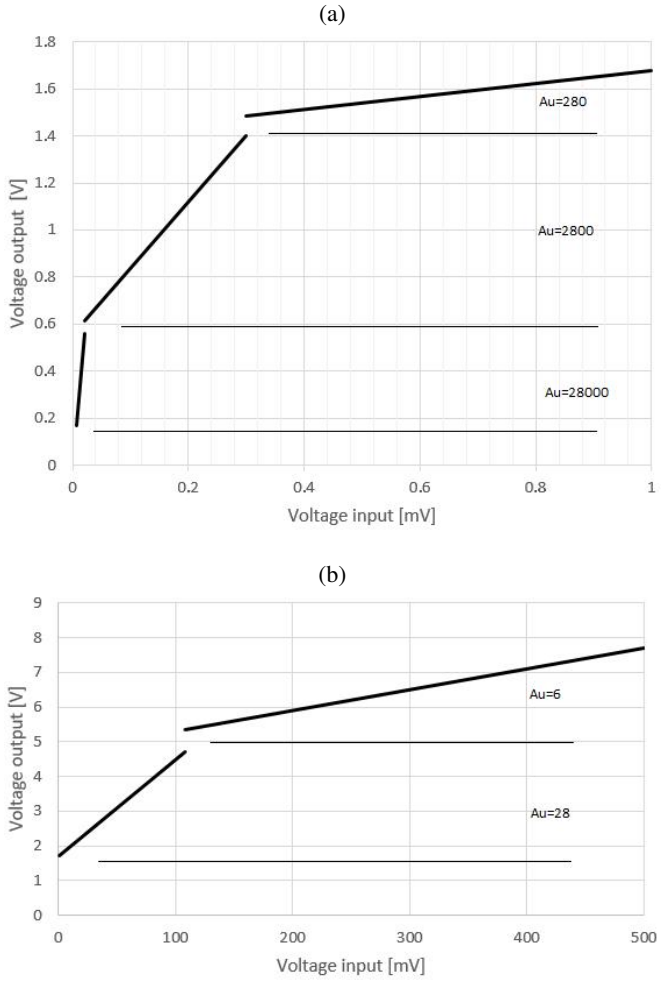

Fig. 6. Output voltage as a function of system input voltage. a) system dynamics for gains of 280, 2800, and 28000; b) system dynamics for gains of 6 and 28 V/V

Table 1
Results of dynamic measurements of the EM receiver

No.	U_{IN} [mV]	Au [V/V]	U_{OUT} [V]	E [V/m]
1	500	6	3.000	5
2	108	6	0.650	1.08
3	108	28	3.000	1.08
4	1	28	0.028	0.01
5	1	280	0.280	0.0
6	0.3	280	0.084	0.003
7	0.3	2800	0.840	0.003
8	0.02	2800	0.056	0.0002
9	0.02	28000	0.56	0.0002
10	0.006	28000	0.168	0.00006

Based on the data in Table 1, the transient characteristic was plotted with the operating thresholds of the automatic gain control AGC system marked (Fig. 6). Based on the measurements, the smallest measurable input signal amplitude, 6 μV, was determined. The maximum signal that can be registered is 500 mV. These values allow the determination of the dynamics of the system, indicated by the formula:

$$D = 20\log\left(\frac{U_{IN\max}}{U_{IN\min}}\right) = 98.41 \text{ dB} \tag{12}$$

A system with dynamics was created, which allows the recording of signals in a large range of dynamic changes. These dynamics allows for the registration of weak EM emission signals (with a small amplitude) with large gains of 28000 and 2800. At the moment of strong mechanical stresses and generation of high amplitude signals by the destroyed rocks, the system registers signals with the lowest gains 6, 28.

5. TESTS OF THE RECEIVER IN THE LABORATORY

An autonomous receiver for measuring spontaneous EM emissions was placed on the laboratory stand in Figure 1. In the jaws of the hydraulic press, samples of hard coal with a base diameter of 2.5 cm and a height of 5 cm were placed. The test samples were obtained from a coal mine from boreholes drilled at the head of the coal seam gallery. An incremental press jaw force of 1 kN/s was applied to the test sample.

Figure 7 shows a representative measurement result obtained by the autonomous EM receiver. The figure shows the time course of the increasing force of the press on the test sample (Fig. 7a) and the recorded in the device memory of the course of the electric component E of the EM field emitted by the tested coal sample. The waveforms were also observed in real time from the RS 232 port available on the receiver.

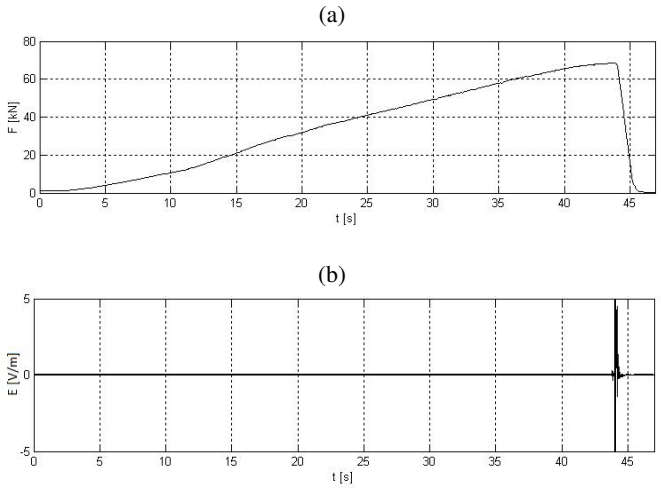

Fig. 7. Electromagnetic emission tests on a laboratory stand. a) time course of the compressive force on the hard coal sample; b) time course of the electric component of the electromagnetic field

Figure 8a shows the first part of the recorded signal from Fig. 7 in the time interval from 18.24 to 18.44 sec. During this time, the observed signal can be stable, and the force acting on the sample is about 30 kN. The E component signal of the field emission recorded by the autonomous receiver reaches an inter-peak energy value of about 0.1 mV/m. This means that the autonomous receiver system operates with a gain equal to the maximum value of Au = 28000 V/V. Figure 8b shows the spectrum of the obtained waveform. The main component of the waveform is the frequency of 50 Hz and its harmonics (50, 100, 150 Hz). The electromagnetic emission coming from the rock subjected to mechanical stress is also quite clearly marked. The dominant frequencies of this emission are about 250 and 500 Hz. This means that microcracks emit low energy in the investigated coal sample. The energy of these pulses is below 30 μV/m.

The obtained waveform subjected to detailed analysis shows high sensitivity of the constructed receiver. In its lower operating range, the autonomous receiver measures weak (with small amplitudes) EM radiation signals coming from antennas. The lowest sensitivity of the measured signal is 6 μV amplitude.

The values of measured energy of disturbance signal from power network reach low values below 50 μV/m. The low values of mains disturbance result from placing the autonomous receiver behind the EM shield and the double bandpass filtering system used in the device.

Figure 9 shows the recorded signal of increased EM emission just before the destruction of the tested coal sample. The force acting on the coal sample reaches a value close to 70 kN. The

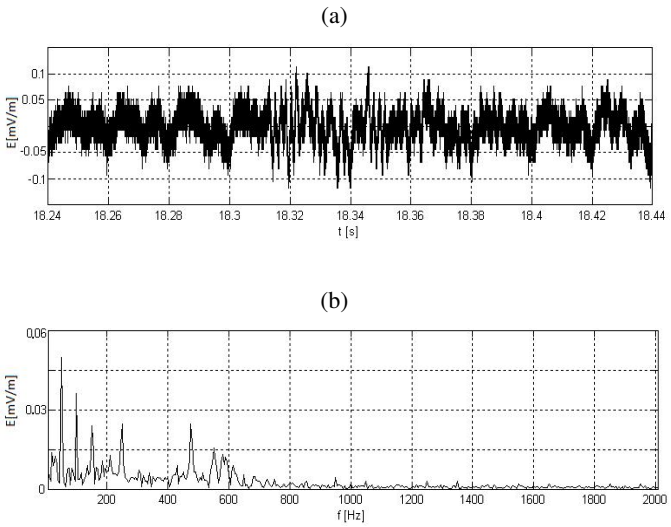

Fig. 8. The first part of the course from Fig. 7 for about 18 s of the test duration. a) time course; b) spectrum of the waveform

sample is not destroyed, but a large micro-crack appears, which causes increased EM emission measured by the E antenna. The increased EM field emission is recorded between 43.8 s and 44 s of the experiment. The signal reaches inter-peak values in the range –0.3 to 0.3 V/m, which means that the receiver circuit is switched between Au = 280 V/V and Au= 28 V/V gain. Due to its increased (anomalous) energy, this signal was recorded in the memory of the autonomous receiver and is available on the SD card. On the card, the algorithm controlling the receiver's operation has recorded the anomalous signal along with 100 ms of the signal preceding the incident. This pulse may be a precursor to the destruction of the rock sample under test.

The determined spectrum for this time interval shows dominant signals in the frequency range from 200 to 800 Hz. Similarly, as for the fragment of the waveform from Fig. 8b, the signal spectrum indicates the highest energy is obtained at a frequency of about 500 Hz.

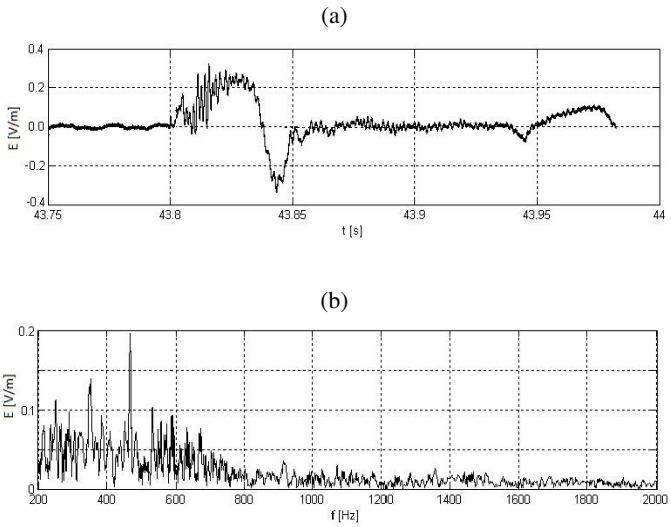

Fig. 9. The second part of the waveform from Fig. 7 at 43.75 to 44 sec. a) time course; b) spectrum of the waveform

Figure 10 shows the third part of the obtained waveform measured at the moment of highest mechanical stress on the tested coal sample. At the critical moment, the force is equal to more than 70 kN. Such a press force causes the destruction of the tested sample in more than 44 s of the experiment. During this time, the highest energy of electromagnetic radiation is spontaneously generated. High up to 5 V/m (anomalous) electric field emission lasts more than 300 ms.

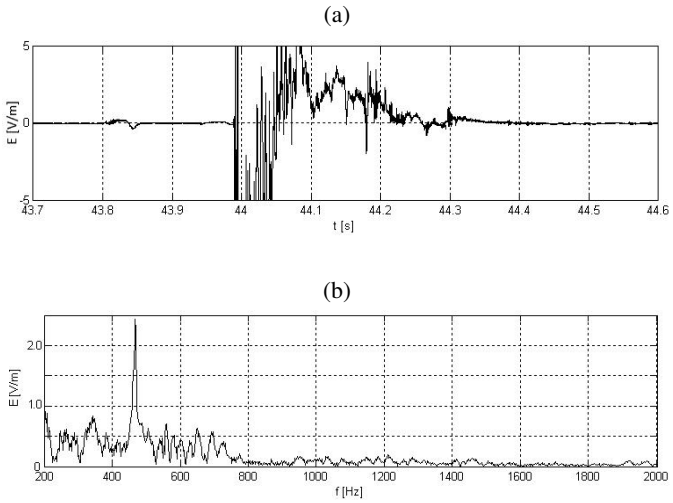

Fig. 10. The third part of the waveform from Fig. 7 at 43.7 to 44.6 sec. a) time course; b) waveform spectrum

During the destruction of the coal sample under test, the autonomous receiver measured the signal change over the largest possible operating range of –5 to 5 V/m. This means that the receiver operated at the lowest gain of Au = 6 V/V. There was also a brief overdrive of the receiver in short pulses. Similarly, as for the waveform in Fig. 9, the algorithm used leads to automatic recording in the receiver's memory of the increased EM emission signal on the SD card. The algorithm recorded the anomalous signal in memory along with 100ms of the preceding waveform.

As in the analyses of the previous results, the spectrum of the obtained signal shows dominant frequencies from 200 to 800 Hz, indicating a distinct 500 Hz signal. The 500 Hz signal has an energy of over 20 V/m.

6. CONCLUSIONS

The design and the algorithm used to control the receiver allows for high dynamic performance of over 98 dB. An Autonomous EM field receiver is characterized by high sensitivity. It allows observation of weak signals emitted by rocks at the level of a single μV. At the same time, it can observe and record strong signals emitted by large microcracks formed in close distance.

The operation of the autonomous receiver was tested in laboratory conditions when a hard coal sample was subjected to increased mechanical stress. The autonomous receiver of EM field emission allowed observation and recording of real signals, and its gain was smoothly switched depending on the energy of the emerging signal. The character and bandwidth of the observed signals were analogous to those of the antennas used in the laboratory. The receiver satisfies all the technical criteria.

The conducted laboratory tests confirmed the formation of spontaneous electromagnetic emission in rock subjected to increased mechanical stress. The spectrum of the resulting signals ranges from hundreds of Hz to single kHz and the energy to ±5 V/m or ±5 A/m. In single pulses exceeding threshold values.

Thanks to its casing, the constructed receiver of electromagnetic field components, the use of an independent power supply and the possibility of recording anomalies in memory can work in mine conditions for observing rock mass stresses. In the prototype version, the receiver works independently as an autonomous device for up to a month. Access to the recorded increased EM signals is possible in real time via RS port and after the measurement period after reading the information from the memory cards.

Further development of research work should allow for the construction of a system, the placement of similar receivers along with mine workings, and connecting them into a common system. The system created based on autonomous receivers can support the existing seismic safety systems, predicting the possibility of mine collapse danger.

REFERENCES

[1] M. Akgun, "Coal mine accidents," *Turk Thorac Journal*, vol. 16, no. 1, pp. s1–s2, 2015, doi: 10.5152/ttd.2015.008.

[2] A. Tubis, S. Werbińska-Wojciechowska, and A. Wróblewski, "Risk assessment methods in mining industry – A systematic review," *Appl. Sci.*, vol. 10, pp.1–34, 2020, doi: 10.3390/app10155172.

[3] J.L.X. Meng, Y. Wang, and Z. Yang, "Prediction of coal seam details and mining safety using multicomponent seismic data: A case history from China," *Geophysics*, vol. 81, no. 5 (September – October), pp. 149–165, 2016, doi: 10.1190/GEO2016-0009.1.

[4] Y. Wang, N. Fu, X. Lu, and Z. Fu, "Application of a new geophone and geometry in tunnel seismic detection," *Sensors*, vol. 19, p. 1246, 2019, doi: 10.3390/s19051246.

[5] R.M. Bhattacharjeeb, A.K. Dasha, and P.S. Paulb, "A root cause failure analysis of coal dust explosion disaster – Gaps and lessons learnt" *Eng. Fail. Anal.*, vol. 111, pp. 1–17, 2020, doi: 10.1016/j.engfailanal.2019.104229.

[6] M. Li *et al.*, "Piezoelectric effect and ignition properties of coal mine roof sandstone deformation and fracture," *Fuel*, vol. 290, pp. 1–9, 2021, doi: 10.1016/j.fuel.2020.120007.

[7] M. Hayakawa, "Earthquake precursor studies in Japan" in *Pre-Earthquake Processes*, Wiley, pp.7–18, 2018, doi: 10.1002/9781119156949.ch2.

[8] B. Kunar, "Risk assessment for disaster management in underground coal mines," *Indian Miner. Ind. J.*, vol. 11, pp. 113–119, 2015.

[9] G.-J. Liu, C.-P. Lu, H.-Y. Wang, P.-F. Liu, and Y. Liu, "Warning method of coal bursting failure danger by electromagnetic radiation," *Shock Vib.*, vol. 2015, p. 583862, 2015, doi: 10.1155/2015/583862.

[10] E. Wang, H. Jia, D. Song, N. Li, and W. Qian, "Use of ultra-low-frequency electromagnetic emission to monitor stress and failure in coal mines," *Int. J. Rock Mech. Min. Sci.*, vol. 70, pp. 16–25, 2014, doi: 10.1016/j.ijrmms.2014.02.004.

[11] A.A. Panfilov, "The results of experimental studies of VLF–ULF electromagnetic emission by rock samples due to mechanical action," *Nat. Hazards Earth Syst. Sci. Discuss.*, vol. 1, pp. 7821–7842, 2013, doi: 10.5194/nhessd-1-7821-2013.

[12] Z. Shijiea, S. Xiaoyuanc, L. Chengwub, X. Xiaoxuan, and X. Zhuang, "The analysis of coal or rock electromagnetic radiation (EMR) signals based on Hilbert-Huang transform (HHT)," *First International Symposium on Mine Safety Science and Engineering*, *Procedia Engineering*, vol. 26, pp. 689–698, 2011.

[13] R. Mydlikowski and K. Maniak, "Measurement of electromagnetic field component emission as a precursor of emerging hazard in coal mines," *J. Telecomm. Inf.Technol.*, vol. 4, pp. 30–35, 2019, doi: 10.26636/jtit.2020.145320.

[14] A. Prałat, K. Maniak, and I. Pompura, "Electromagnetic phenomena in landslides," *Acta Geodynamica and Geomaterialia*, vol. 2, no. 3, pp. 131–138, 2005.

[15] V. Frid, "Calculation of electromagnetic radiation criterion of rockburst hazard forecast in coal mines," *Pure Appl. Geophys.*, vol. 158, pp. 931–944, 2001, doi: 10.1007/PL00001214.

[16] V. Frid and K. Vozoff, "Electromagnetic radiation induced by mining rock failure," *Int. J. Coal Geol.*, vol. 64, pp. 57–65, 2005, doi: 10.1016/j.coal.2005.03.005.

[17] D. Lin-ming, L. Cai-ping, M. Zong-long, and G. Ming-shi, "Prevention and forecasting of rock burst hazards in coal mines," *Min. Sci. Technol.*, vol. 19, pp. 585–591, 2009, doi: 10.1016/S1674-5264(09)60109-5.

[18] S.G. O'Keefe and D.Thiel, "Electromagnetic emissions during rock blasting," *Geophys. Res. Lett.*, vol. 18, no. 5, pp. 889–892, 1991, doi: 10.1029/91GL01076.

[19] P. Xiong *et al*., "Identification of electromagnetic pre-earthquake perturbations from the DEMETER data by machine learning," *Remote Sens.*, vol. 12, pp. 1–27, 2020, doi: 10.3390/rs12213643.

[20] A. Erturk and D.J. Inman, *Piezoelectric Energy Harvesting*, First Edition, John Wiley & Sons, Ltd. Published 2011, pp. 343–344.

[21] M. Krumbholz, M. Bock, S. Burchardt, U. Kelka, and A. Vollbrecht, "A critical discussion of the electromagnetic radiation (EMR) method to determine stress orientations within the crust," *Solid Earth*, vol. 3, pp. 401–414, 2012, doi: 10.5194/sed-4-993-2012.

[22] A. Rabinovitch, V. Frid, D. Bahat ,and J. Goldbaum, "Decay mechanism of fracture induced electromagnetic pulses," *J. Appl. Phys.*, vol. 93, no. 9, pp 5085–5090, 2003, doi: 10.1063/1.1562752.

[23] A. Rabinovitch, V. Frid, and D. Bahat, "Surface oscillations. A possible source of fracture induced electromagnetic radiation," *Tectonophysics*, vol. 431, pp 15–21, 2007, doi: 10.1016/j.tecto.2006.05.027.

[24] A. Takeuchi and H. Nagahama, "Electric dipoles perpendicular to a stick-slip plane," *Phys. Earth Planet. Inter.*, vol. 155, pp. 208–218, 2006, doi: 10.1016/j.pepi.2005.12.010.

[25] P. Koktavy and J. Sikula, "Physical model of electromagnetic emission in solids," *Proc. 26th Eur. Conf. Acous. Emission Testing EWGAE 2004*, *Berlin*, *Germany*, 2004, pp. 899–904.

[26] S.K. Sharma, R. Kiran, A. Kumar, V.S. Chauhan, and R. Kumar, "A theoretical model for the electromagnetic radiation emission from hydrated cylindrical cement paste under impact," *J. Phys. Commun.*, vol. 2, no. 3, pp. 1–12, 2018,

[27] D. Miedzińska, T. Niezgoda, E. Małek, and D. Zasada, "Study on coal microstructure for porosity levels assessment," *Bull. Pol. Acad. Sci. Tech. Sci.*, vol. 61, no. 2, pp. 409–505, 2013, doi: 10.2478/bpasts-2013-0049.

[28] F. Zhao, Y. Li, Z. Ye, Y. Fan, S. Zhang, H. Wang, and Y. Liu, "Research on acoustic emission and electromagnetic emission characteristics of rock fragmentation at different loading rates," *Shock Vib.*, vol. 2018, p. 4680879, 2018, doi: 10.1155/2018/4680879.

[29] Z. Loni, H. Espinosa, and D. Thiel, "Insulated wire fed floating monopole antenna for coastal monitoring," *Radioengineering*, vol. 27, no. 1, pp. 127–133, 2018, doi: 10.13164/re.2018.0127.

[30] V. Dyo, T. Ajmal, B. Allen, D. Jazani, and I. Ivanov, "Design of a ferrite rod antenna for harvesting energy from medium wave broadcast signals," *J. Eng.*, vol. 2013, no. 12, pp. 89–96, 2013, doi: 10.1049/joe.2013.0126.

[31] T. Bolton and M.B. Cohen, "Optimal design of electrically-small loop receiving antenna," *Prog. Electromagn. Res. C*, vol. 98, pp. 155–169, 2020, doi: 10.2528/PIERC19090911.

[32] U. Tietze, Ch. Schenk, and E. Gamm, *Electronic Circuits–Handbook for Design and Application*, 2nd Edition. Springer, 2011, pp. 787–841.